THE JOURNAL OF PHYSICAL CHEMISTRY Letters

Letter

pubs.acs.org/JPCL

Self-Induced Surfactant Transport along Discontinuous Liquid–Liquid Interfaces

David K. N. Sinz, Myroslava Hanyak, and Anton A. Darhuber*

Mesoscopic Transport Phenomena Group, Department of Applied Physics, Eindhoven University of Technology, Postbus 513, 5600MB Eindhoven, The Netherlands

Supporting Information

ABSTRACT: While the Marangoni-stress-driven spreading of surfactants along continuous fluid interfaces is a well-studied problem, we demonstrate experimentally that swift and efficient surfactant transport can also occur along discontinuous interfaces. We used chemical surface patterning to create arrays of discrete drops and liquid bridges immersed inside a second immiscible liquid. Surface-active compounds introduced at one end of the linear array are transported along the array via surfactant-induced interfacial convection at a rate by far exceeding diffusion. We believe this mechanism to be relevant to the application of surfactants in enhanced oil recovery, where oil–water interfaces are likely to be discontinuous. Marangoni flows can provide access to dead-end pores and low-permeability regions that are otherwise bypassed by conventional pressure-driven waterfloods.

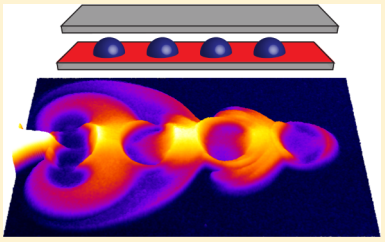

SECTION: Liquids; Chemical and Dynamical Processes in Solution

Due to their surface-active nature, spatially nonuniform distributions of surfactants induce flows at fluid interfaces that in turn transport the surfactants and cause them to spread. This phenomenon has been studied extensively in the context of liquid–air[1−14] and liquid–liquid interfaces.[15−22] The technological applications of these flows range from detergency,[23] drug delivery,[24] lab-on-a-chip applications,[25−27] and inkjet printing[28] to extraction and mass transfer processes,[16−20,29−31] emulsions,[32,33] and enhanced oil recovery.[33−42]

In an oil reservoir, oil–water interfaces are likely not continuous over long distances. The oil or the aqueous phase may reside in disconnected regions that are predetermined, for example, by the morphology and wettability of the surrounding rock pores. Motivated by the question of whether surfactant-induced Marangoni flows could provide an efficient transport mechanism along such *discontinuous* interfaces, we fabricated linear arrays of droplets and liquid bridges that are immersed in an immiscible and continuous liquid bulk-phase. Deposition of surfactant at one end of an array causes Marangoni flows along the liquid–liquid interfaces, which induce convection patterns in both phases. We show that surfactant is transported across sizable interface discontinuities and along the array of droplets and liquid bridges. We believe that this self-induced transport along a discontinuous interface is a conceptually novel phenomenon of potentially high technological relevance.

We consider an elementary model geometry that captures the essence of the phenomenon and facilitates quantitative understanding of the process on the level of a single pore. The experimental implementation of our discontinuous interface system is illustrated in Figure 1a–d. The surface of a hydrophobized glass substrate is chemically patterned into an array of hydrophilic circles of diameter D = 3 mm and spacing w_{gap} using the procedure described in ref 13. Droplets of the polar liquid ethylene glycol (EG) with center height h_D are deposited onto these hydrophilic spots. A coverglass plate is maintained parallel at a well-defined distance by means of glass spacers with a thickness of h_s = 1 mm on both sides of the droplet array. The remaining cavity between the substrates is filled with dodecane via capillary imbibition.

Following dodecane imbibition, a 10 μL drop of a surfactant (Triton X-15) solution in dodecane, which also contains a dissolved dye (Oil Red), is deposited near one end of the immersed droplet array using a Hamilton microsyringe. The weight-averaged concentration w_{X15} of the surfactant solutions in dodecane ranged from 0.16 to 25%. Utilizing the presence of the dye, we monitored the spatial distribution of the surfactant by measuring light absorption in a transmission configuration. The refractive indices of the two liquids are almost equal, such that artifacts originating from light refraction at liquid–liquid interfaces are negligible.

When the front of the injected surfactant solution reaches the first EG droplet, the interfacial tension is locally reduced, and the resulting interfacial tension gradients give rise to flows along and around the droplet-oil interface. Figure 1e–h shows experimental images taken at different stages of this spreading process. For better visualization, the recorded grayscale was inverted such that regions with a high surfactant and dye concentration appear bright. In Figure 1e, the surfactant distribution 0.1 s after contact with the first droplet is shown. The Marangoni flows along the liquid–liquid interface induce a complex convection pattern in the surrounding continuous oil

Received: February 8, 2013
Accepted: March 12, 2013
Published: March 12, 2013

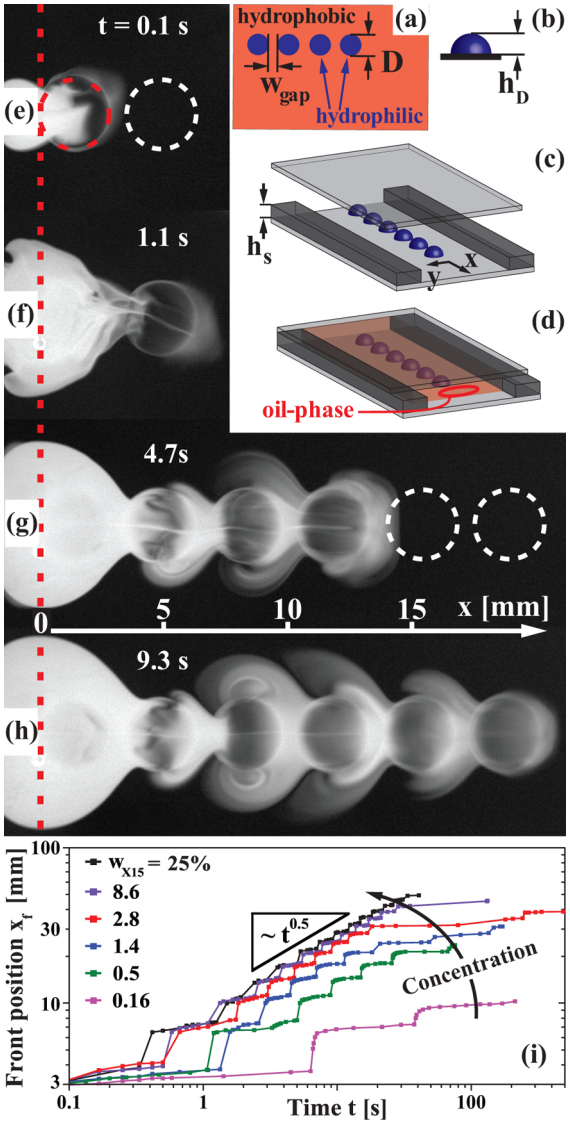

Figure 1. (a) Chemical surface pattern on the hydrophobic bottom substrate, consisting of a linear array of hydrophilic circles of diameter D and spacing w_{gap}. (b) EG droplets of center height h_D are deposited on the hydrophilic spots. (c) Glass spacers of thickness h_s = 1 mm on both sides of the droplet array maintain a parallel coverglass plate at a well-defined distance. (d) Capillary imbibition of dodecane. (e–h) Background-corrected and gray scale inverted transmission images of different stages of a spreading experiment with parameter values h_D = 420 μm, D = 3 mm, and w_{gap} = 0.5 mm. After the front of the surfactant solution contacts the first droplet (dashed red line in panel e), the front propagates along the droplet array. (i) Front position as a function of time for various surfactant concentrations and parameters h_D = 660 μm, D = 3 mm, and w_{gap} = 0.5 mm.

phase, which transports the surfactant to the next droplet with an initially surfactant-free interface, as shown in Figure 1f. The spreading process continues in this fashion, and the surfactant is transported through the oil phase along the array, as illustrated in Figure 1f–h.

This spreading process is many orders of magnitude faster than diffusion of surfactant through the oil phase. As the leading edge of the surfactant distribution advances from droplet to droplet, the concentration at the front progressively decreases. Concurrently, the surfactant-induced interfacial tension gradients at the liquid–liquid interfaces decrease, and the front propagation slows down. However, the convective flow in the oil-phase surrounding the droplets that were already passed by the front continues though with decreasing magnitude. A consequence of this continued convection is the widening of the surfactant distribution around the droplets in the y-direction.

Figure 1i illustrates the surfactant front propagation for various concentrations w_{X15} and constant drop height h_D = 660 μm and gap width w_{gap} = 0.5 mm. The terraced appearance of the curves is a result of the different transport rates along the droplet interfaces and across the gaps between adjacent droplets. Along the liquid–liquid interface, the propagation proceeds rapidly with the speed of the induced Marangoni flow. Across the gaps, the transport mechanism is bulk convection and diffusion of surfactant-rich continuous phase in a nonunidirectional velocity field that decays away from the droplet interfaces into the oil-phase.

Two distinct regimes are evident in the front propagation data for w_{X15} = 2.8% (red curve in Figure 1i). Initially, for times $t \lesssim 20$ s, the data is globally well approximated by a power-law relation $x_f \sim t^{\alpha}$ with a spreading exponent of $\alpha \approx 0.5$, while for later times α appears to decrease. The onset of this transition in the spreading exponent occurs earlier for lower concentrations. In the data set for w_{X15} = 25% (black curve in Figure 1i), no transition is observed within the duration of the experiment.

Figure 2 illustrates the effect of a variation in the drop height h_D. The experimental images in Figure 2a,b correspond to h_D =

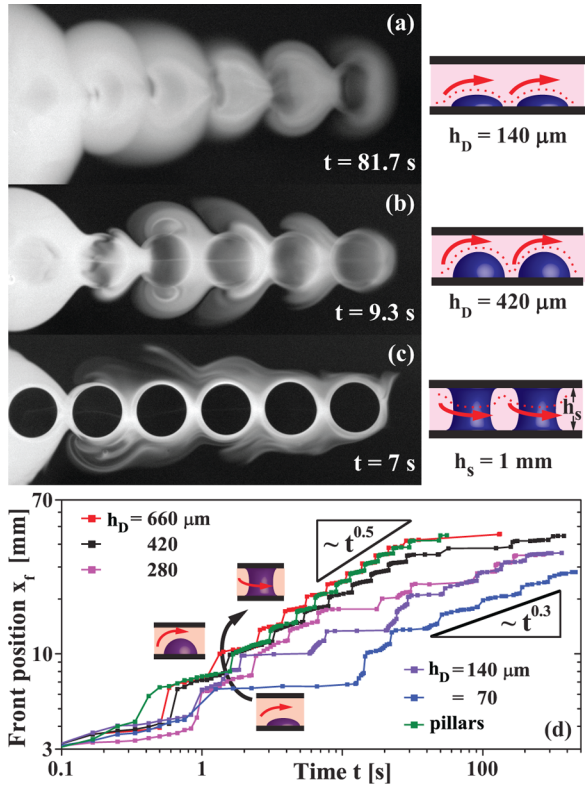

Figure 2. (a–c) Background-corrected and gray scale inverted transmission images obtained at different stages of spreading experiments with droplets of height (a) h_D = 140 μm and (b) 420 μm as well as (c) liquid bridges of height h_s = 1 mm, nominal footprint diameter D = 3 mm and gap width w_{gap} = 0.5 mm. (d) Front position x_f as a function of time for various droplet heights h_D and parameter values w_{X15} = 8.6%, D = 3 mm, and w_{gap} = 0.5 mm.

dx.doi.org/10.1021/jz400287x | J. Phys. Chem. Lett. 2013, 4, 1039–1043

140 and 420 μm. For the experiment presented in Figure 2c, chemically patterned substrates were used for both the bottom as well as the top substrate, and EG drops were deposited on both. Upon contact, the drops coalesced and formed liquid bridges with a height equal to the plate spacing h_s = 1 mm. While for the droplet arrays, the convection of surfactant rich oil-phase occurred predominantly above the droplets, for the liquid bridges, the surfactant rich oil-phase is convected around the pillars, as illustrated in the diagrams on the right side of Figure 2(a–c). In Figure 2d, the surfactant front position x_f is plotted as a function of time for droplets of different heights h_D as well as for the pillar array. The gap width and concentration were kept constant in these experiments at w_{gap} = 0.5 mm and w_{X15} = 8.6%, respectively.

For droplets of h_D = 420 and 660 μm as well as the liquid bridges of 1 mm height the surfactant front propagated at comparable rates. For smaller droplet heights, the propagation rate tends to decrease with decreasing droplet height. The overall propagation rate is well approximated by a power law relation $x_f \sim t^{\alpha}$ with an exponent $\alpha \approx 0.5$ for pillars and droplets of height $h_D \geq 420$ μm (red, green, and black curves in Figure 2d). For the lowest two values of h_D = 70 and 140 μm, however, the average propagation rate is governed by an exponent $\alpha \approx 0.3$ in the late stage (blue and violet curves in Figure 2d).

The effect of a variation of the spacing between adjacent droplets w_{gap} is illustrated in Figure 3. The experimental images in Figure 3a–d correspond to w_{gap} = 0.5, 1, 2, and 3 mm and different times when the surfactant front in each experiment had reached a position of $x_f \approx 24$ mm.

It is evident that with increasing spacing w_{gap}, the lateral extension δy of the surfactant-rich zone around the individual droplets slightly increased. The time evolution of the front position x_f is presented in Figure 3e. While the propagation appears qualitatively similar for all four cases, the absolute spreading rate decreased with increasing drop spacing.

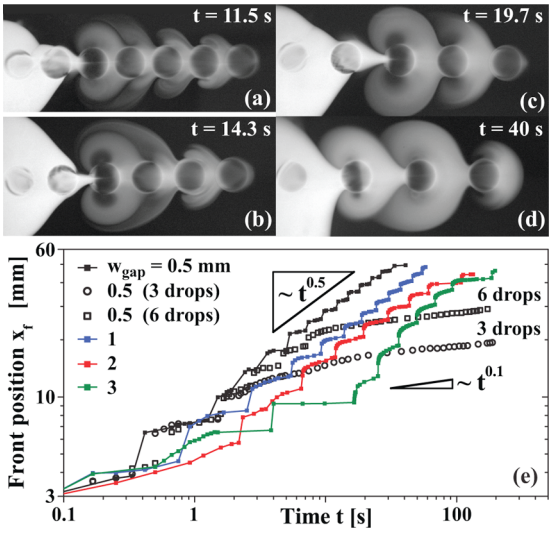

Figure 3. (a-d) Background-corrected and grayscale-inverted transmission images obtained at different stages during spreading experiments along droplet arrays with gap widths (a) w_{gap} = 0.5 mm, (b) 1 mm, (c) 2 mm, and (d) 3 mm and parameter values h_D = 660 μm and D = 3 mm. (e) Surfactant front position x_f as a function of time for spreading along droplet arrays with different gap-spacings w_{gap} and parameter values h_D = 660 μm, w_{X15} = 25%, D = 3 mm. Filled symbols refer to long arrays, the end of which is not reached during an experiment. Open symbols correspond to data obtained with short arrays comprising only three (circles) and six droplets (squares) with a spacing of w_{gap} = 0.5 mm.

The open symbols in Figure 3e correspond to experiments with short arrays consisting of only three (circles) and six droplets (squares). These data illustrate the mechanism behind the surfactant propagation over discontinuous interfaces. While the front propagation rate decreased after passing the last droplet in the array, the Marangoni flow along the droplet array did not cease. This not only causes the propagation of the front to the next *clean* droplet in an array, but also drives continued transport of surfactant-rich oil-phase from the location of initial deposition over the already contacted droplets to the surfactant front.

We attribute this prolonged flow along the droplet array, i.e., over droplets already passed by the surfactant front (see Video 3 in the Supporting Information), to two main factors. The high Peclet number $Pe \equiv Uh_s/D_s \approx 10^6$, where U is a typical velocity and D_s the diffusion coefficient of the surfactant in the continuous phase, induces the formation of concentration boundary layers in the immediate vicinity of the liquid–liquid interfaces. Moreover, in our system, there occurred no net flow of the continuous phase, which is characteristic of dead-end pores or zones surrounded by regions of low permeability in porous materials. This necessitates a nonunidirectional velocity profile in response to the interfacial Marangoni flows. The interplay of the concentration boundary layers with this recirculatory flow leads to a net desorption of surfactant away from the liquid–liquid interfaces. This occurs until the surfactant concentration is homogenized along the array, even if the surfactant is insoluble in the discontinuous phase. Different phases of the recirculatory flow around droplet #4 in an array with D = 3 mm, w_{gap} = 0.5 mm, and h_D = 660 μm are visualized in Figure 4a–e.

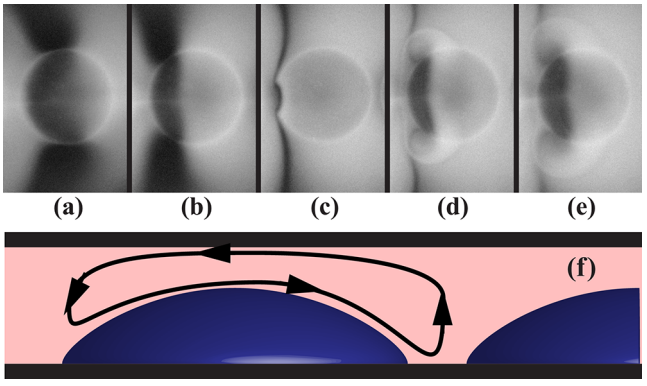

Figure 4. (a–e) False-color transmission images of the surfactant distribution around the fourth droplet in an array with parameters D = 3 mm, w_{gap} = 0.5 mm and h_D = 660 μm at times (a) t = 38.2, (b) 50.9, (c) 62.5, (d) 67.3, and (e) 69.0 s after the surfactant front reached the first drop. (f) Qualitative sketch of a streamline of the recirculatory flow around a droplet.

In summary, we presented systematic experimental evidence that the spreading of surfactants is not limited to continuous interfaces. We investigated the transport of a surfactant along linear arrays of droplets or liquid bridges of a polar liquid submersed in a continuous and immiscible oil-phase. The surfactant is transported through the continuous phase by the

dx.doi.org/10.1021/jz400287x | J. Phys. Chem. Lett. 2013, 4, 1039–1043

flow field induced by surfactant concentration gradients and corresponding Marangoni-stresses at the liquid−liquid interfaces. We studied the influence of various parameters on the spreading dynamics such as the surfactant concentration and the height of and spacing between adjacent droplets. A phase-inverted system, in which the aqueous-phase would be continuous, would behave in the same fashion upon introduction of a water-soluble surfactant.

We believe this newly discovered phenomenon to be especially relevant in the context of surfactant-assisted enhanced oil recovery. Under reservoir conditions, an uninterrupted, i.e., continuous, interface between the oil and aqueous phases is unlikely to occur over long distances. Surfactant-induced Marangoni flows could provide an efficient mechanism to create flow in dead-end pore geometries or low-permeability regions that are bypassed by and thus inaccessible to pressure-driven flows typical for waterfloods. These flows could be employed not only to transport the surfactant itself, but also to deliver functional materials, such as wettability modifiers[43−47] into these conventionally inaccessible reservoir regions, which in turn may increase crude oil recovery rates.[48,49] Two prerequisites of this transport mechanism, however, are that the liquid−liquid interfaces are sufficiently mobile and that the rates of surfactant adsorption and desorption are sufficiently rapid.

EXPERIMENTAL METHODS

All chemicals were purchased from Sigma Aldrich and, with the exception of dodecane, used as received: EG (product number 324558), Triton X-15 (product number X15-500 ML), Oil Red O (product number O0625), and high-purity-grade dodecane (purity >99%, product number 221104). Using a syringe filter, undissolved dye was removed prior to surfactant addition to obtain a particle-free solution. A sketch of the molecular structure of Triton X-15 is provided in the Supporting Information. Pendant drop tensiometer measurements showed that the interfacial tension (IFT) of dodecane against deionized water was time dependent and significantly lower than literature values, which scatter around $\gamma_{O/W}(25°C) \approx 53$ mN/m.[50−52] This indicates the presence of surface active impurities,[50−54] which we eliminated by repeated addition of basic aluminum oxide (product number 199443) and its subsequent removal via vacuum filtration. After purification, the IFT values were within the range of scatter for the different reported literature values and remained constant over the period of 1 h, which by far exceeds the duration of our experiments.

The absorption measurements were performed with an AVT Pike CCD camera, a 0.33× telecentric lens with a field of view of 28.5 mm and a Thorlabs HPLS-30-04 lightsource in a transmission geometry.

ASSOCIATED CONTENT

Supporting Information

The chemical structure of Triton X-15 as well as three videos illustrating the dynamics of the surfactant transport process along one-dimensional arrays of liquid bridges and droplets, respectively. This material is available free of charge via the Internet http://pubs.acs.org.

AUTHOR INFORMATION

Corresponding Author

*E-mail: A.A.Darhuber@tue.nl.

Notes

The authors declare no competing financial interest.

ACKNOWLEDGMENTS

The authors thank Steffen Berg and Axel Makurat from Shell International Exploration and Production (Rijswijk, The Netherlands) for the inspiring collaboration. The authors gratefully acknowledge that this research is supported partially by the Dutch Technology Foundation STW, the applied science division of NWO, and the Technology Program of the Ministry of Economic Affairs.

REFERENCES

(1) Hoult, D. P. Oil Spreading on the Sea. *Annu. Rev. Fluid Mech.* **1972**, *4*, 341−368.
(2) Foda, M.; Cox, R. G. The Spreading of Thin Liquid Films on a Water−Air Interface. *J. Fluid Mech.* **1980**, *101*, 33−51.
(3) Camp, D. W.; Berg, J. C. The Spreading of Oil on Water in the Surface-Tension Regime. *J. Fluid Mech.* **1987**, *184*, 445−462.
(4) Borgas, M. S.; Grotberg, J. B. Monolayer Flow on a Thin Film. *J. Fluid Mech.* **1988**, *193*, 151−170.
(5) Troian, S. M.; Wu, X. L.; Safran, S. A. Fingering Instability in Thin Wetting Films. *Phys. Rev. Lett.* **1989**, *62*, 1496−1499.
(6) Gaver, D. P.; Grotberg, J. The Dynamics of a Localized Surfactant on a Thin Film. *J. Fluid Mech.* **1990**, *213*, 127−148.
(7) Halpern, D.; Grotberg, J. B. Dynamics and Transport of a Localized Soluble Surfactant on a Thin Film. *J. Fluid Mech.* **1992**, *237*, 1−11.
(8) Jensen, O. E. The Spreading of Insoluble Surfactant at the Free Surface of a Deep Fluid Layer. *J. Fluid Mech.* **1995**, *293*, 349−378.
(9) Dussaud, A. D.; Troian, S. M.; Harris, S. R. Fluorescence Visualization of a Convective Instability Which Modulates the Spreading of Volatile Surface Films. *Phys. Fluids* **1998**, *10*, 1588−1596.
(10) Warner, M. R. E.; Craster, R. V.; Matar, O. K. Pattern Formation in Thin Liquid Films with Charged Surfactants. *J. Colloid Interface Sci.* **2003**, *268*, 448−463.
(11) Matar, O. K.; Craster, R. V. Dynamics of Surfactant-Assisted Spreading. *Soft Matter* **2009**, *5*, 3801−3809.
(12) Narayanan, R. *Interfacial Processes and Molecular Aggregation of Surfactants*; Springer: Berlin, 2008.
(13) Sinz, D. K. N.; Hanyak, M.; Zeegers, J. C. H.; Darhuber, A. A. Insoluble Surfactant Spreading Along Thin Liquid Films Confined by Chemical Surface Patterns. *Phys. Chem. Chem. Phys.* **2011**, *13*, 9768−9777.
(14) Hanyak, M.; Sinz, D. K. N.; Darhuber, A. A. Soluble Surfactant Spreading on Spatially Confined Thin Liquid Films. *Soft Matter* **2012**, *8*, 3660−3671.
(15) Magome, N.; Yoshikawa, K. Nonlinear Oscillation and Ameba-like Motion in an Oil/Water System. *J. Phys. Chem.* **1996**, *100*, 19102−19105.
(16) Kovalchuk, N. M.; Vollhardt, D. Nonlinear Spontaneous Oscillations at the Liquid/Liquid Interface Produced by Surfactant Dissolution in the Bulk Phase. *J. Phys. Chem. B* **2005**, *109*, 22868−22875.
(17) Lavabre, D.; Pradines, V.; Micheau, J.-C.; Pimienta, V. Periodic Marangoni Instability in Surfactant (CTAB) Liquid/Liquid Mass Transfer. *J. Phys. Chem. B* **2005**, *109*, 7582−7586.
(18) Kovalchuk, N. M.; Vollhardt, D. Oscillation of Interfacial Tension Produced by Transfer of Nonionic Surfactant through the Liquid/Liquid Interface. *J. Phys. Chem. C* **2008**, *112*, 9016−9022.
(19) Szpakowska, M.; Plocharska-Jankowska, E.; Nagy, O. B. Molecular Mechanism and Chemical Kinetic Description of Nitrobenzene Liquid Membrane Oscillator Containing Benzyldimethyltetradecylammonium Chloride Surfactant. *J. Phys. Chem. B* **2009**, *113*, 15503−15512.
(20) Nanzai, B.; Funazaki, T.; Igawa, M. Threshold for Spontaneous Oscillation in a Three-Phase Liquid Membrane System Involving Nonionic Surfactant. *J. Phys. Chem. B* **2010**, *114*, 11778−11783.

(21) Zhao, G.; Pumera, M. Liquid−Liquid Interface Motion of a Capsule Motor Powered by the Interlayer Marangoni Effect. *J. Phys. Chem. B* **2012**, *116*, 10960−10963.
(22) Berg, S. Marangoni-Driven Spreading Along Liquid−Liquid Interfaces. *Phys. Fluids* **2009**, *21*, 032105.
(23) Cutler, W. G.; Kissa, E. *Detergency: Theory and Technology*; Marcel Dekker: New York, 1986.
(24) Gaver, D. P.; Grotberg, J. Droplet Spreading on a Thin Viscous Film. *J. Fluid Mech.* **1992**, *235*, 399−414.
(25) Kralj, J. G.; Schmidt, M. A.; Jensen, K. F. Surfactant-Enhanced Liquid−Liquid Extraction in Microfluidic Channels with Inline Electric-Field Enhanced Coalescence. *Lab Chip* **2005**, *5*, 531−535.
(26) Diguet, A.; Guillermic, R.-M.; Magome, N.; Saint Jalmes, A.; Chen, Y.; Yoshikawa, K.; Baigl, D. Photomanipulation of a Droplet by the Chromocapillary Effect. *Angew. Chem., Int. Ed.* **2009**, *48*, 9281−9284.
(27) Sinz, D. K. N.; Darhuber, A. A. Self-Propelling Surfactant Droplets in Chemically-Confined Microfluidics - Cargo Transport, Drop-Splitting and Trajectory Control. *Lab Chip* **2012**, *12*, 705−707.
(28) Hanyak, M.; Darhuber, A. A.; Ren, M. Surfactant-Induced Delay of Leveling of Inkjet-Printed Patterns. *J. Appl. Phys.* **2011**, *109*, 074905.
(29) Adachi, M.; Harada, M.; Nishita, R.; Shioi, A. Extraction Kinetics of Small Charged Molecules in Water-in-Oil Microemulsion/Brine System. *J. Phys. Chem.* **1995**, *99*, 8722−8729.
(30) Williams, C. L.; Bhakta, A. R.; Neogi, P. Mass Transfer of a Solubilizate in a Micellar Solution and Across an Interface. *J. Phys. Chem. B* **1999**, *103*, 3242−3249.
(31) Sczech, R.; Eckert, K.; Acker, M. Convective Instability in a Liquid−Liquid System Due to Complexation with a Crown Ether. *J. Phys. Chem. A* **2008**, *112*, 7357−7364.
(32) Tabor, R. F.; Lockie, H.; Mair, D.; Manica, R.; Chan, D. Y. C.; Grieser, F.; Dagastine, R. R. Combined AFM-Confocal Microscopy of Oil Droplets: Absolute Separations and Forces in Nanofilms. *J. Phys. Chem. Lett.* **2011**, *2*, 961−965.
(33) Pereira, J. C.; Delgado Linares, J.; Scorzza, C.; Rondon, M.; Rodriguez, S.; Salager, J.-L. Breaking of Water-in-Crude Oil Emulsions. 4. Estimation of the Demulsifier Surfactant Performance to Destabilize the Asphaltenes Effect. *Energy Fuels* **2011**, *25*, 1045−1050.
(34) deZabala, E. F.; Vislocky, J. M.; Rubin, E.; Radke, C. J. A Chemical Theory for Linear Alkaline Flooding. *SPE J. (Soc. Pet. Eng.)* **1982**, *22*, 245−258.
(35) Lake, L. W. *Enhanced Oil Recovery*; Prentice-Hall: Upper Saddle River, NJ, 1989.
(36) Morrow, N. R. *Interfacial Phenomena in Petroleum Recovery*; Marcel Dekker: New York, 1990.
(37) Taylor, K. C.; Schramm, L. L. Measurement of Short-Term Low Dynamic Interfacial Tensions: Application to Surfactant Enhanced Alkaline Flooding in Enhanced Oil Recovery. *Colloids Surf.* **1990**, *47*, 245−253.
(38) Farajzadeh, R.; Andrianov, A.; Zitha, P. L. J. Investigation of Immiscible and Miscible Foam for Enhancing Oil Recovery. *Ind. Eng. Chem. Res.* **2010**, *49*, 1910−1919.
(39) Hirasaki, G. J.; Miller, C. A.; Puerto, M. Recent Advances in Surfactant EOR. *SPE J. (Soc. Pet. Eng.)* **2012**, *16*, 889−907.
(40) Ash, P. A.; Bain, D. B.; Matsubara, H. Wetting in Oil/Water/Surfactant Systems. *Curr. Opin. Colloid Interface Sci.* **2012**, *17*, 196−204.
(41) Chen, I.-C.; Akbulut, M. Nanoscale Dynamics of Heavy Oil Recovery Using Surfactant Floods. *Energy Fuels* **2012**, *26*, 7176−7182.
(42) Liu, Q.; Yuan, S.; Yan, H.; Zhao, X. Mechanism of Oil Detachment from a Silica Surface in Aqueous Surfactant Solutions: Molecular Dynamics Simulations. *J. Phys. Chem. B* **2012**, *116*, 2867−2875.
(43) Rosen, M. J.; Wang, H.; Shen, P.; Zhu, Y. Ultralow Interfacial Tension for Enhanced Oil Recovery at Very Low Surfactant Concentrations. *Langmuir* **2005**, *21*, 3749−3756.
(44) Bain, C. D. Penetration of Surfactant Solutions Into Hydrophobic Capillaries. *Phys. Chem. Chem. Phys.* **2005**, *7*, 3048−3051.
(45) Somasundaran, P.; Zhang, L. Adsorption of Surfactants on Minerals for Wettability Control in Improved Oil Recovery Processes. *J. Petroleum Sci. Eng.* **2006**, *52*, 198−212.
(46) Zhang, D. L.; Liu, S.; Puerto, M.; Miller, C. A.; Hirasaki, G. Wettability Alteration and Spontaneous Imbibition in Oil-Wet Carbonate Formations. *J. Pet. Sci. Eng.* **2006**, *52*, 213−226.
(47) Hammond, P. S.; Unsal, E. Spontaneous and Forced Imbibition of Aqueous Wettability Altering Surfactant Solution into an Initially Oil-Wet Capillary. *Langmuir* **2009**, *25*, 12591−12603.
(48) Wasan, D. T.; Nikolov, A. D. Spreading of Nanofluids on Solids. *Nature* **2003**, *423*, 156−159.
(49) Morrow, N.; Buckley, J. Improved Oil Recovery by Low-Salinity Waterflooding. *JPT, J. Pet. Technol.* **2011**, *63*, 106−113.
(50) Demond, A. H.; Lindner, A. S. Estimation of Interfacial Tension Between Organic Liquids and Water. *Environ. Sci. Technol.* **1993**, *27*, 2318−2331.
(51) Goebel, A.; Lunkenheimer, K. Interfacial Tension of the Water/*n*-Alkane Interface. *Langmuir* **1997**, *13*, 369−372.
(52) Zeppieri, S.; Rodríguez, J.; López De Ramos, A. L. Interfacial Tension of Alkane + Water Systems. *J. Chem. Eng. Data* **2001**, *46*, 1086−1088.
(53) Georgiadis, A.; Maitland, G.; Trusler, J. P. M.; Bismarck, A. Interfacial Tension Measurements of the (H_2O + *n*-Decane + CO_2) Ternary System at Elevated Pressures and Temperatures. *J. Chem. Eng. Data* **2011**, *56*, 4900−4908.
(54) Fricke, M.; Sundmacher, K. Mass Transfer Model of Triethylamine across the *n*-Decane/Water Interface Derived from Dynamic Interfacial Tension Experiments. *Langmuir* **2012**, *28*, 6803−6815.